Density functional study of the actinide nitrides

Raymond Atta-Fynn and Asok K. Ray*
Physics Department, University of Texas at Arlington, Arlington, Texas 76019, USA
(Received 22 February 2007; revised manuscript received 14 July 2007; published 4 September 2007)

The full-potential all-electron linearized augmented plane wave plus local orbital method, as implemented in the suite of the software WIEN2K, has been used to systematically investigate the structural, electronic, and magnetic properties of the actinide compounds AnN (An=Ac, Th, Pa, U, Np, Pu, and Am). The theoretical formalism used is the generalized gradient approximation to density functional theory with the Perdew-Burke-Ernzerhof exchange-correlation functional. Each compound has been studied at the nonmagnetic, ferromagnetic, antiferromagnetic configurations, all with and without spin-orbit coupling (SOC). The structural parameters, bulk moduli, densities of states, and charge distributions have been computed and compared to available experimental data and other theoretical calculations published in the literature. Our total energy calculations clearly indicate that AcN, ThN, and PaN are nonmagnetic, while the ground states of UN, NpN, PuN, and AmN are found to be ferromagnetic. The influence of SOC in the actinide nitrides is found to be significant. The nature of the interactions between the actinide metals and nitrogen atom and the implications on $5f$ electron delocalization and localization are discussed in detail.

DOI: 10.1103/PhysRevB.76.115101 PACS number(s): 71.20.−b, 71.27.+a

I. INTRODUCTION

Actinides and compounds thereof continue to be highly complex and challenging areas of research from both scientific and technological points of view.[1–6] Actinide nitrides are very promising advanced fuel materials for fast breeder reactors. They are also target materials for the transmutation of plutonium and minor actinides in fast reactor cores and in accelerator driven systems. In fact, actinide nitrides are under investigation for the fuels of the future fast neutron fission reactors developed in Forum Generation IV. The high density of the nitride fuel brings out more excess neutrons and has a higher potential to transmute the long lived fission products. If one considers the breeding ratio, appropriate thermophysical properties (high thermal conductivity, high melting point, and high fuel density), chemical compatibility with the Na coolant, and reprocessing feasibility, actinide nitrides appear to be a compromise between oxide and metal fuels. In fact, the thermal conductivity of PuN is usually in the range of 11–13 W/m K, that of UN being 20–23 W/m K compared to the values of 3–5 W/m K for UO_2 and PuO_2 in the range of 800–1600 K. Actinide mononitrides are typically brittle refractory materials with a melting point usually greater than 2000 °C. For uranium nitride, the melting point is around 2850 °C and the density is around 14.32 g/cm^3. As mentioned before, they have a higher energy neutron spectrum, respond better to demands of actinide burning, and have a long core life.[7,8] Also, higher thermal conductivity provides a margin of fuel melting and gives a negative feedback because of the Doppler reactivity in an unprotected loss of flow accidents. Nitrides, in fact, provide a direct path toward the self-consistent nuclear energy system, defined as a system which satisfies four objectives: energy generation, fuel breeding, confinement of the minor actinides and radioactive fission products, and nuclear reactor safety.

As a continuation of our continued study of actinide surface chemistry and physics,[9] this work is concerned with detailed fundamental *ab initio* electronic structure studies of actinide nitrides. Such studies, though rather important as implied above, are relatively scarce in the literature. In contrast to metallic fuels, actinide nitrides form an isostructural series of mononitrides (AnN) with a simple rocksalt-type structure. These systems are AcN, ThN, PaN, UN, NpN, PuN, and AmN. In fact, the actinide mononitrides AnN (An=Ac, Th, Pa, U, Np, Pu, and Am) fall under a large family of actinide compounds with a rocksalt-type structure, which includes the monocarbides AnC, monopnictides AnX (X=N, P, As, Sb, and Bi), monochalcogenides AnX (X=S, Se, and Te), and their solutions. The UN phase diagram actually indicates that there are three thermodynamically stable phases below 400 °C, namely, UN, α-U_2N_{3+x} (existing in the range $UN_{1,54}$ and $UN_{1.75}$), and UN_2. Also of interest are nitride systems such as $(U_{0.8}Pu_{0.2})N$, (Np,Pu)N, Th_3N_4, β-U_2N_3, (Pu,Zr)N, (Pu,Am)N, and (Pu,Ac,Zr)N, with Ac representing one of the minor actinides, Np, Am, and Cm. Zr is added as a diluent, and typically all these fuels form single-phase solid solutions under normal irradiation conditions. There are outstanding questions of interest in relation to these nitrides. One question, similar to the persistent question of magnetism in Pu, for example,[9] relates to magnetism in actinide nitrides. Experimentally, UN undergoes antiferromagnetic ordering with the Néel temperature at 53 K. A small ordered moment and a moderate γ coefficient of the low-temperature specific heat indicates an itinerant character of UN magnetism. In highly distorted thin films (low-temperature deposition), UN appears to exhibit a weak Pauli paramagnetism. In this regard, real structure and magnetic properties of bulk actinide nitrides and thin films need to be carefully examined, both theoretically and experimentally. Another question relates to the character of the $5f$ states in actinide nitrides. One photoelectron spectroscopy study of PuN indicates that the $5f$ states appear in the vicinity of the Fermi level, exhibiting the same type of features as in Pu metals, and the $5f$ states are essentially delocalized. The third question relates to the corrosion of actinides by water. There are, for example, uncertainties about the stability of

UN in water. Some studies suggest that UN is stable in contact with boiling water and water at 300 °C, while other studies suggest that UN undergoes hydrolysis by superheated steam. In fact, x-ray photoemission spectroscopy (XPS) results indicate that a freshly fractured surface of UN quickly converts to UO_2 on exposure to liquid water or water vapor at ambient temperature. For the sake of brevity, we first comment only on *some* of the published literature.

Brooks and Kelly[10] performed linear-muffin-tin-orbital (LMTO) energy-band calculations in the atomic sphere approximation for UC and UN. They found that spin-orbit coupling induced a predominant orbital magnetic moment antiparallel to the spin moment for UN. The overall results, such as the magnetic form factor, pressure dependence of the moment, and presence of large magnetic anisotropy, indicated an itinerant electron behavior, though the authors indicated that more careful analysis are needed to distinguish between localized and itinerant $5f$ magnetism. Using a relativistic linear-muffin-tin-orbital (RLMTO) method, Brooks[10] also studied the trends in the lattice parameters of the actinide nitrides from self-consistent LMTO, RLMTO, and spin-polarized LMTO calculations and interpreted the results in terms of metallic $5f$-$5f$ and covalent cation $5f$–anion $2p$ contributions to the calculated equations of state. Large magnetovolume effects were found for NpN-AmN. Spin-orbit splitting increased the atomic volumes of NpN-AmN, and the density of states at the Fermi level was found to be basically of $5f_{5/2}$ character for the paramagnetic ground states of UN-AmN. Using a semiempirical potential, Kurosaki *et al.*[11] performed molecular dynamics (MD) simulations of the actinide nitrides (ThN, UN, NpN, and AmN) in the 300–2800 K temperature range and in the pressure range of 0.1 MPa–1.5 GPa to investigate their physical and thermodynamical properties. A Morse-type potential function was added to the Busing-Ida-type potential to describe the ionic interactions, and the authors concluded that MD simulations could successfully describe the physical properties of actinide nitrides. Petit *et al.*[12] calculated the electronic structure of AmN using self-interaction-corrected local-spin-density (SIC-LSD) approximation. They concluded that the properties of AmN are well described by a trivalent (f^6) electronic configuration for Am ion. In a follow-up study, using the same approximation, they concluded that the localized $5f^3$ configuration (with the rest of the $5f$ states forming a band) is the most probable ground state of PuN. However, this conclusion was questioned by Havela *et al.*[13] from their reactive sputtering studies of Pu in an Ar atmosphere with a variable concentration of N. They found that the $5f$ emission dominating closer to the Fermi level displayed characteristics similar to the Pu metal and that the $5f$ states can be assumed to be essentially delocalized. In a follow-up study, Rafaja *et al.*[13] reported the structure and magnetic properties of UN thin films prepared by reactive vapor deposition at temperatures between −200 and +400 °C, providing a large variety of microstructures, and observed the evolution of the $5f$ magnetism as a function of deviation from the ideal crystallinity. At low temperatures, the long-range antiferromagnetism is suppressed and a ferromagnetic component is induced, producing a cluster glass type of ordering and, eventually, UN indicates a weak Pauli paramagnetism. Marutzky *et al.*[14] reported optical measurements from 1 to 10 eV and magneto-optical measurements from 1 to 5 eV on a UN single crystal. Compared to the results for uranium monopnictides, they found an increased hybridization of the U ($5f$) states with the U ($6d$) and N ($2p$) states. Sheng[15] applied the linear free energy correlation model of Sverjensky and Molling,[16] which correlates the standard free formation energy with thermodynamics of the corresponding metal cations to the actinide mononitrides, with the actinides treated as trivalent cations. The calculated free energies of formation and experimental data for some of the nitrides were found to be in fairly good agreement. Recently, Sedmidubsky *et al.*[8] calculated the enthalpies of formation of the actinide mononitride series using a full-potential linear augmented plane wave plus local orbital basis (FP-LAPW+lo)[17] with the generalized gradient approximation[18] within the framework of density functional theory (DFT). They observed a linear decrease in the enthalpies of formations from AcN to AmN, which was attributed to the stabilizing effect of the Madelung term as the bonding becomes more ionic. Except for AcN and PaN, for which lattice parameters were optimized, the basic structural parameters of all the other nitrides were taken from a database[19] and ferromagnetic spin-polarized calculations at the scalar relativistic level were performed. The authors obtained good agreement with experimental data for UN and NpN enthalpies of formation but not for PuN and ThN. The authors speculated that the increasing role of electron correlations might have played a role for PuN. More recently, Shein *et al.*[20] have studied the electronic structure properties of cubic ThC, ThN, and ThO using the FP-LAPW+lo method within the generalized gradient approximation (GGA)-DFT approximation. For perfectly stoichiometric ThN, they found good agreement with experimental values for the lattice constant, bulk modulus, and specific heat coefficient. They also noted that the bonding behavior of the ThX (X=C, N, and O) phases is a linear combination of covalent, ionic, and metallic characters. The local density approximation with Hubbard potential and spin-orbit coupling (LDA+U+SOC) method has been used by Shorikov *et al.*[21] to investigate the electronic structures and magnetic state of the α and δ phases of metallic Pu and its compounds. For PuN, an f^5 configuration with a sizable magnetic moment was found. Ghosh *et al.*[22] studied the ground state and optical properties of the americium monopnictides, AmX (X=N, P, As, Sb, and Bi), using the local density approximation LDA and LDA+U methods. They found that LDA predicted a pseudogaplike behavior in AmN while LDA+U predicted a semiconducting behavior with a real gap of 192 meV in AmN. Obviously, there are disagreements and discrepancies in the published literature about the actinide nitrides, and our study, we believe, is an attempt to treat all nitrides on an equal footing at different configurations with and without SOC.

II. COMPUTATIONAL METHODOLOGY

As mentioned in the abstract, we have carried out density functional calculations for the actinide nitrides using the all-electron FP-LAPW+lo method, as implemented in the all-

electron WIEN2K code[17] in the GGA-DFT approximation[18] at the nonmagnetic (NM), ferromagnetic (FM), and antiferromagnetic (AFM) configurations, all with and without SOC. One purpose of doing both levels of theory is to investigate spin-orbit coupling effects on the structural, magnetic, and electronic properties. In the WIEN2K code, core states are treated fully relativistically, while the valence states are treated at the scalar relativistic level. However, relativistic effects for the valence electrons was included, not by solving the Dirac equation but via a second variational step,[23] in which the effects of SOC are treated perturbatively using the scalar relativistic eigenstates as the basis within a given energy window. For this work, eigenstates with energies below 4.5 Ry are used. As mentioned by Kunes *et al.*,[24] this cutoff usually implies that a limited number of the low-lying eigenfunctions are used. Relativistic $p_{1/2}$ orbitals have been included to account for the finite character of the $p_{1/2}$ wave function at the nucleus.[24] The quantization axis for the magnetic SOC calculations was [001]. Muffin-tin radii for the actinide atoms have been chosen as follows: 2.5 a.u. for Ac and Th, 2.4 a.u. for Pa, U, Np, Pu, and Am, and 1.7 a.u. for N. The parameter $R_{\mathrm{MT}}K_{\mathrm{max}}=8$, where R_{MT} is the smallest muffin radius and K_{max} is the truncation for the modulus of reciprocal lattice vector, was used for the plane waves expansion of the wave function in the interstitial region (this corresponds to a kinetic energy cutoff of 22.15 Ry).

To study type-I AFM configurations, consisting of alternating spin-up and spin-down ferromagnetic sheets along the [001] magnetic axis, we used a unit cell with four atoms per cell. For UN, we also used a unit cell with eight atoms per cell to study type-II AFM configuration, which consists of AFM order in the three cubic directions. In the results to follow, we will discuss the two configurations in detail. Reciprocal space integration in the first Brillouin zone was performed on a grid of 1000 k points. Convergence of total energies with respect to the number of k points and K_{max} has been thoroughly checked. The total energy and the charge difference $\int(\rho_n-\rho_{n-1})dr$ were simultaneously converged to terminate the self-consistent iterations. Convergence criteria for the energy and charge difference were 0.01 mRy and 0.0001, respectively. Energies of the free atoms, which were used for the calculations of cohesive energies of the solids, were computed by placing atoms in a box of 15 Å sides and only the Γ k point was used, with the muffin-tin sphere R_{MT} being the same as in the calculations for the solid. However, to ensure that the atomic energies are well converged, the parameter for determining the size of basis set, $R_{\mathrm{MT}}K_{\mathrm{max}}$, was gradually increased until the change in the atomic energies was $\sim$1 mRy, yielding $R_{\mathrm{MT}}K_{\mathrm{max}}=9.5$.

We hasten to point out that while the LDA and GGA to DFT has been known to work well for the light actinides with delocalized 5f electrons, *sometimes* it does not yield the right predictions for actinides with localized electrons with respect to *certain* electronic structure properties. For example, experiments predict the absence of magnetic moments in δ-Pu, but antiferromagnetic spin configuration is needed for DFT-GGA/local spin density approximation (LSDA) to predict the right equilibrium atomic volume.[9] As such, the predicting power of DFT-GGA with FP-LAPW +lo with regards to the magnetic and electronic properties of the systems with localized 5f electrons (particularly Pu and Am) *may* not be *entirely* reliable. This is because LSDA/GGA assumes delocalized electrons and the exchange-correlation functional term does not account for the narrow 5f bands in a proper way due to the poor treatment of on-site electron-electron interactions.[12] One possibility is to use the self-interaction correction scheme,[25] which treats itinerant and localized electrons on an equal footing by including an explicit energy contribution for an electron to localize.[26] The FP-LAPW+lo method used in this work does have the LDA+U (SIC) scheme implemented in it at the expense of the introduction of an additional empirical parameter U, and it is not clear or possible at this point to estimate the effects, *if any*, of this on the results and discussions to follow. We will, of course, compare our lattice parameters and associated electronic and geometric structure properties with other results using GGA,[8,20] LSDA,[10] LDA+SIC,[12] and LDA+U,[22] as reported in the literature.

III. RESULTS AND DISCUSSIONS

In Table I, the calculated equilibrium lattice constants and bulk moduli obtained from fits to Murnaghan's equation of state[27] are presented. The known experimental lattice constants of the actinide mononitrides are 9.74, 9.24, 9.25, 9.27, and 9.44 a.u. for ThN, UN, NpN, PuN, and AmN, respectively.[20,28,29] It can be readily observed that the atomic volume contracts with the gradual filling of the 5f electrons up to U and begins to expand slowly from Np to Pu, and finally a significant increase occurs in the atomic volume of Am. Comparing the predicted lattice constants in Table I to the respective experimental lattice constants, we find a good agreement with ThN and UN at all theoretical levels, with the maximum percentage error being 0.6. Moreover, the equilibrium lattice constants of 10.45 and 9.37 a.u. obtained for AcN and PaN, respectively, are in excellent agreement with the recent theoretical values of 10.42 and 9.37 a.u. obtained by Sedmidubsky *et al.*,[8] while the equilibrium lattice constant of 9.79 for ThN is in exact agreement with a recent calculation by Shein *et al.*[20] From NpN to AmN, the calculated lattice constants at the AFM, AFM+SOC, FM, and FM+SOC levels of theory are also in good agreement with experiments, the maximum percentage error being all less than unity. For NpN-AmN, significant discrepancies (greater than 1%) are observed at the NM (and NM+SOC) levels of theory, with AmN showing the largest departure (5%) from the experimental value. This tends to indicate that unlike ThN and UN, a spin-polarized theory is needed to accurately predict the lattice parameters of NpN to AmN. Our equilibrium lattice constant of 9.29 a.u. for PuN is in much better agreement with the experimental value of 9.27 a.u. compared to the value of 9.69 a.u. obtained by Petit *et al.*[12] Also, our equilibrium lattice constant of 9.40 and a value of 9.44 a.u. obtained by Petit *et al.* agree well with the experimental value of 9.44 a.u. for AmN, while the value of 9.12 a.u. obtained by Ghosh *et al.*[22] underestimates the experimental value by 3.8%. Further comparisons of lattice constants are summarized in Fig. 1, where we show a plot of the lattice constants obtained for our lowest energy structures, the

TABLE I. Optimized lattice constants a (in a.u) and bulk moduli B (in GPa). Δa and ΔB are the respective percentage error of the lattice constants and bulk moduli from experimental values.

	Theory	a (a.u.)	Δa (%)	B (GPa)	ΔB (%)
AcN	NM	10.47		100	
	AFM	10.47		101	
	FM	10.47		100	
	NM+SOC	10.45		100	
	AFM+SOC	10.45		99	
	FM+SOC	10.45		99	
ThN	NM	9.79	0.5	178	1.7
	AFM	9.79	0.5	178	1.7
	FM	9.79	0.5	178	1.7
	NM+SOC	9.78	0.4	162	−7.4
	AFM+SOC	9.78	0.4	170	−2.9
	FM+SOC	9.78	0.4	162	−7.4
PaN	NM	9.37		223	
	AFM	9.37		223	
	FM	9.37		224	
	NM+SOC	9.35		205	
	AFM+SOC	9.35		200	
	FM+SOC	9.36		210	
UN	NM	9.18	−0.6	227	
	AFM	9.20	−0.4	213	
	FM	9.20	−0.4	209	
	NM+SOC	9.20	−0.4	229	
	AFM+SOC	9.21	−0.3	221	
	FM+SOC	9.21	−0.3	219	
NpN	NM	9.06	−2.1	228	
	AFM	9.21	−0.4	177	
	FM	9.22	−0.3	151	
	NM+SOC	9.13	−1.3	209	
	AFM+SOC	9.19	−0.6	195	
	FM+SOC	9.19	−0.6	183	
PuN	NM	9.00	−2.9	218	
	AFM	9.30	0.3	155	
	FM	9.36	1.0	1.48	
	NM+SOC	9.11	−1.7	192	
	AFM+SOC	9.26	−0.1	160	
	FM+SOC	9.29	0.2	147	
AmN	NM	8.97	−5.0	211	
	AFM	9.42	−0.2	130	
	FM	9.45	0.1	145	
	NM+SOC	9.12	−3.4	186	
	AFM+SOC	9.36	−0.8	141	
	FM+SOC	9.40	−0.4	145	

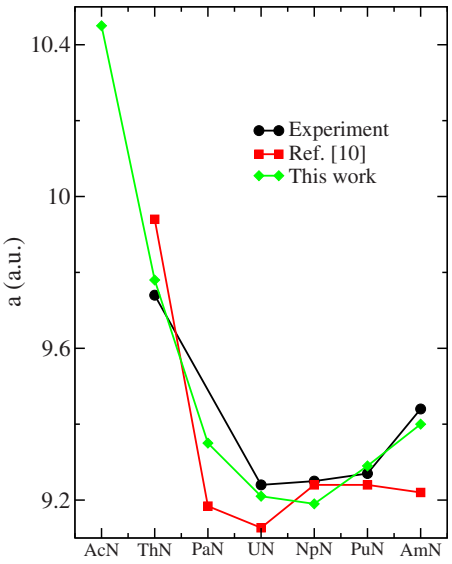

FIG. 1. (Color online) Lattice constants (in a.u.) of the actinide mononitrides.

known experimentally measured lattice constants, and that of Brooks.[10] For ThN, Brooks' results indicate a 2.1% overestimation of the experimental value, whereas our result overestimate the experimental value by 0.4%. For UN, our lattice constant and Brooks' are underestimated by 0.3% and 1.2%, respectively. Brook's results for NpN are almost in exact agreement with experiment, whereas ours show a 0.6% contraction. Both results for PuN show a small expansion of about 0.2%, while the results for AmN show contractions of 0.4% in our case and 2.3% in Brook's results. Overall, the lattice constants obtained in both cases agree reasonably well with experiment. Next, we discuss the trends in the bulk moduli reported in Table I. For AcN-UN, the reported values are fairly consistent at each theoretical level, and the respective percentage errors from experimental data, available only for ThN, vary from 1.7% to 7.4%. Compared to Brooks' results (shown in parentheses), the bulk moduli in gigapascal corresponding to our lowest energy structures are 99, 170 (174), 200 (217), 219 (214), 183 (200), 147 (194), and 145 (177) for AcN, ThN, PaN, UN, NpN, PuN, and AmN, respectively. The results for ThN, PaN, UN, and NpN are in fair agreement with each other, while significant discrepancies are observed for PuN and AmN. However, as the discussions in the next section clearly indicate, AcN to PaN are nonmagnetic, and the very slightly differing values in the lattice constants and bulk moduli can be attributed to "numerical noise." In fact, for ThN (the only compound for which experimental data are available), the percentage difference between our largest and smallest lattice constants is 0.1.

In the first column of Table II, the total energy difference ΔE for each compound from their respective ground states is listed for each theoretical level. Here, $\Delta E > 0$ indicates instability. First of all, it is clearly evident, as mentioned before, that with and without SOC, the ground states of AcN to PaN are clearly nonmagnetic, with the energy differences attributed to numerical noise. For each compound, however, the

TABLE II. Total energy difference relative to the ground state ΔE (mRy/unit cell), spin-polarization energies E_{SP} (mRy/unit cell), spin-orbit coupling energies E_{SO} (mRy/unit cell), and total spin magnetic moments μ_s (μ_B/unit cell) for the actinide mononitrides at different theoretical levels.

	Theory	ΔE (mRy/unit cell)	E_{SP} (mRy/unit cell)	E_{SO} (mRy/unit cell)	μ_s (μ_B/unit cell)
AcN	NM	285.784			
	AFM	285.794	−0.010		0.00
	FM	285.791	−0.007		0.00
	NM+SOC	0.130		285.654	
	AFM+SOC	0.186	−0.056	285.608	0.00
	FM+SOC	0.000	0.130	285.791	0.00
ThN	NM	336.245			
	AFM	336.245	0.000		0.00
	FM	336.245	0.000		0.00
	NM+SOC	0.260		335.985	
	AFM+SOC	0.000	0.260	336.245	0.00
	FM+SOC	0.002	0.258	336.243	0.00
PaN	NM	385.740			
	AFM	385.740	0.000		0.00
	FM	385.737	0.003		0.00
	NM+SOC	0.223		385.517	
	AFM+SOC	0.000	0.223	385.740	0.00
	FM+SOC	0.109	0.114	385.628	0.00
UN	NM	446.168			
	AFM	443.706	2.642		0.00
	FM	440.696	5.472		1.23
	NM+SOC	4.433		441.735	
	AFM+SOC	1.073	3.360	442.633	0.00
	FM+SOC	0.000	4.433	440.696	0.96
NpN	NM	535.332			
	AFM	505.212	30.120		0.00
	FM	499.024	36.308		3.11
	NM+SOC	20.803		514.529	
	AFM+SOC	3.569	17.234	501.643	0.00
	FM+SOC	0.000	20.803	499.024	2.45
PuN	NM	646.606			
	AFM	553.425	93.181		0.00
	FM	542.775	103.831		4.85
	NM+SOC	37.813		608.793	
	AFM+SOC	3.7915	34.022	549.634	0.00
	FM+SOC	0.000	37.813	542.775	4.26
AmN	NM	792.877			
	AFM	600.031	192.846		0.00
	FM	583.163	209.714		6.00
	NM+SOC	85.125		707.752	
	AFM+SOC	10.201	74.924	589.83	0.00
	FM+SOC	0.000	85.125	572.962	5.64

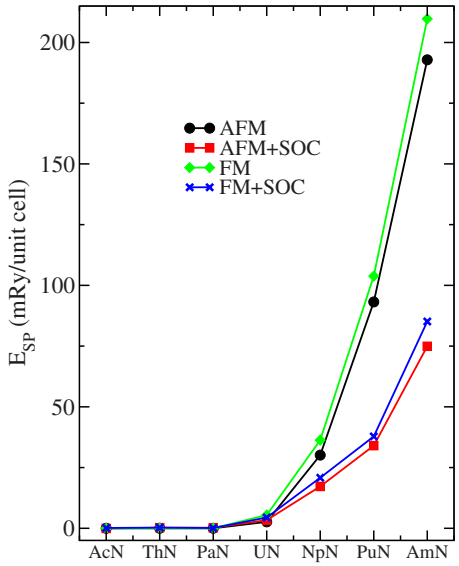

FIG. 2. (Color online) Spin-polarization energy of the actinide mononitrides.

total energy is lowered significantly with the inclusion of spin-orbit coupling, implying that the effects of SOC is large and cannot be ignored. From the results reported in Table II, we see that for UN, NpN, PuN, and AmN, the ground states are clearly FM. The energy differences stemming from spin-polarized and spin-orbit coupling effects are listed in Table II. To facilitate our discussions, we have pictorially represented the spin-polarization energy E_{SP} in Fig. 2 and the spin-orbit coupling energy E_{SO} in Fig. 3. Here, E_{SP} is defined as $E_{NM(+SOC)}-E_{FM(+SOC)/AFM(+SOC)}$ and E_{SO} is defined as $E_{NM/AFM/FM}-E_{NM+SOC/AFM+SOC/FM+SOC}$. In Fig. 2, we clearly observe no spin-polarization effects on the energy from AcN to PaN, as expected. From UN to AmN, E_{SP} increases smoothly. It is worth noting that spin polarization lowers the

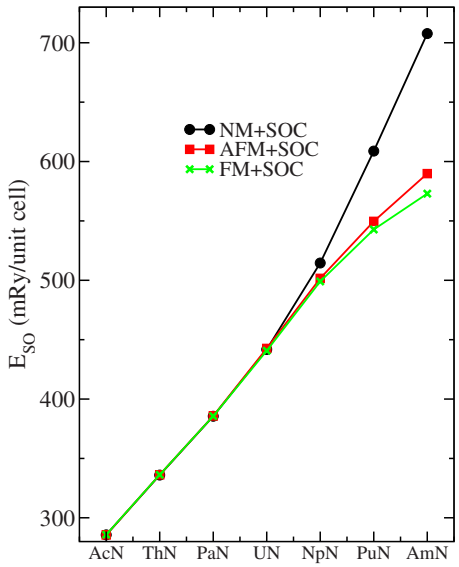

FIG. 3. (Color online) Spin-orbit coupling energy of the actinide mononitrides.

total energy of the FM and AFM configurations more than it does for FM+SOC and AFM+SOC. In Fig. 3, we observe that the individual SOC energies for AcN, ThN, PaN, and UN are nearly constant at the three NM+SOC, AFM+SOC, and FM+SOC levels. From NpN to AmN, we observe pronounced spin-orbit coupling energy-lowering effects at the NM+SOC level, followed by AFM+SOC and FM+SOC.

As stated earlier, for UN, we also studied a larger cell (eight atoms per unit cell) to study type-II AFM ordering, i.e., AFM ordering in all three cubic directions. This unit cell also naturally accommodates type-I AFM ordering, i.e., alternating spin-up and spin-down ferromagnetic sheets along [001]. We show, as an example, the result for an eight-atom UN unit cell and compare with the results obtained with the four-atom unit cell results for the lattice constants and bulk moduli in Table III and the energy differences in Table IV. Upon examining Table III, we first observe that the lattice constants at the various theoretical levels used for the cells agree quite well, with the differences attributed to numerical inaccuracies. Also, a comparison of the AFM type-II structural properties with AFM type-I properties for the eight atom cell indicates basically identical results. Next, we look at the energy differences listed in Table IV. If we compare the energy differences at the different theoretical levels used for both cells, we see that the total energy differences are typically less than a millirydberg. The same is true for the spin-polarization energy, spin-orbit coupling energy, as well as the total and site-projected spin magnetic moments. Also, the results indicate that without SOC, the total energies of AFM type-II and AFM type-I configurations are basically degenerate, while with SOC the total energy for the AFM type-I configuration is 0.838 mRy/unit cell lower than that for the AFM type II. The total energies of the ground states for the four-atom and eight-atom cells at the FM+SOC level are −56 276.131 084 and −56 276.133 284 Ry/unit cell, respectively.

In Fig. 4, we show plots of the cohesive energies per unit cell E_{cohes} for each solid for the lowest energy structures in comparison to recent spin-polarized GGA calculations using same code reported in Ref. 8. Here, we define E_{cohes} as $1/N_U[N_U E_{An}+N_U E_N-E_{AnN}]$, where N_U is the number of AnN pairs inside the unit cell, E_{An} and E_N are, respectively, the isolated atomic energies of the actinide and nitrogen, and E_{AnN} is the total energy of AnN. With this definition, positive cohesive energy indicates binding and negative cohesive energy otherwise. Figure 4 indicates an increase in cohesive energies from AcN to PaN and a linear decrease from PaN to AmN, while the results of Sedmidubsky *et al.*[8] indicate a nonlinear decrease from ThN to AmN. A possible explanation for the differences in the magnitudes of the cohesive energies is the difference in computational approaches used. For example, in Ref. 8, only the lattice constants of AcN and PaN were optimized and all calculations were done using spin-polarized GGA (with SOC neglected), while in our case all lattice constants were optimized at all levels. The high cohesive energy of PaN indicate a significant contribution of $5f$ and $6d$ to covalent bonding, with the contributions of $5f$ electrons to covalent bonding decreasing from PaN-AmN.[8]

In Table II, we have listed the net spin magnetic moments of the solids. In Table V, the site-projected moment S, orbital

TABLE III. Comparison of lattice constants a and bulk moduli B for a four-atom cell and an eight-atom cell for UN. The numbers in parentheses denote the percentage error of the quantity from experimental values.

	Four-atom cell		Eight-atom cell	
Theory	a (a.u.)	B (GPa)	Lattice constant (a.u.)	Bulk modulus (GPa)
NM	9.18 (−0.6%)	227	9.20 (−0.4%)	229
AFM2			9.21 (−0.3%)	216
AFM1	9.20 (−0.4%)	213	9.21 (−0.3%)	216
FM	9.20 (−0.4%)	209	9.22 (−0.2%)	214
NM+SOC	9.20 (−0.4%)	229	9.20 (−0.4%)	223
AFM2+SOC			9.21 (−0.3%)	229
AFM1+SOC	9.21 (−0.3%)	221	9.21 (−0.3%)	222
FM+SOC	9.21 (−0.3%)	219	9.21 (−0.3%)	235

moment L, and total moment J for each actinide with a nonzero magnetic moment corresponding to lowest energy structures (i.e., UN, NpN, PuN, and AmN at the FM+SOC level of theory) are reported. All the moments in Table V are computed within the muffin-tin and, therefore, exclude interstitial contributions. Orbitals moments were computed inside the muffin tin for cases with SOC but without orbital polarization. As stated earlier, the ground states of AcN, ThN, and PaN are clearly nonmagnetic. For ThN, this is in agreement with the experimentally observed paramagnetic ground state[30] and a recent theoretical calculation[20] using the same code. As mentioned before, experimental data indicate that magnetic ordering in UN occurs at the Néel temperature T_N=53 K to an antiferromagnetic type-I structure.[31–34] Our results predict a ferromagnetic structure for UN at 0 K, with the total spin magnetic moment in the unit cell for the lowest energy FM+SOC structure to be $0.96\mu_B$. From Table V, we observe a cancellation of the projected spin moment by the orbital moment for U. The vanishing total moment for U is a clear indication of the delocalized nature of the U $5f$ electrons in UN. Next, we consider the magnetic structure of NpN. Experimental studies have shown that NpN is a ferromagnet with Curie temperature T_C=87 K.[35] Our FM+SOC results reported for NpN clearly agree with the experimentally observed FM ground state. From Table II, we see that the total spin magnetic moment in the cell is $2.45\mu_B$. Again, from Table V, we see a cancellation of the site-projected spin moment of Np by the orbital moment; hence, just like U, the almost vanishing total moment in the muffin tin signifies $5f$ delocalization in NpN. Neutron diffraction experiments for PuN showed no long-range order or magnetic moments larger than $0.25\mu_B$.[36] AFM ordering at T_N=13 K was suggested on the basis of a maximum in the magnetic susceptibility and specific heat.[36] According to another magnetic susceptibility curve, PuN is a Curie-Weiss paramagnet with an effective moment $\mu_{\text{eff}}=1.08\mu_B$/Pu.[37] However, our results clearly predict a ferromagnetic ground state. From Table II, the total spin magnetic moment of the cell is $4.26\mu_B$. From Table V the total Pu magnetic moment is $1.81\mu_B$, indicating localized $5f$ electron moments. The predicted magnetic moment for Pu agrees with the value of $2.06\mu_B$ obtained by Shorikov *et al.*[21] Detailed theoretical calculations[38] and photoemission experiments on Am, AmN, AmSb, and Am_2O_3 films[39] clearly indicate that Am has localized and nonpolarized $5f^6$ electrons that form a closed relativistic subshell. In fact, Gouder *et al.*[39] found that in all four systems, the $5f$

TABLE IV. Comparisons of total energy differences relative to the ground state ΔE (mRy/unit cell), spin-polarization energies E_{SP} (mRy/unit cell), and spin-orbit coupling energies E_{SO} (mRy/unit cell) for the four-atom and eight-atom cells of UN.

	Four-atom cell			Eight-atom cell		
Theory	ΔE (mRy/unit cell)	E_{SP} (mRy/unit cell)	E_{SO} (mRy/unit cell)	ΔE (mRy/unit cell)	E_{SP} (mRy/unit cell)	E_{SO} (mRy/unit cell)
NM	446.168			446.145		
AFM2				443.501	2.644	
AFM1	443.706	2.642		443.503	2.643	
FM	440.696	5.472		440.450	5.695	
NM+SOC	4.433		441.7345	5.610		440.535
AFM2+SOC				2.025	3.585	441.4763
AFM1+SOC	1.073	3.360	442.633	1.187	4.424	442.316
FM+SOC	0.000	4.433	440.6960	0.000	5.610	440.450

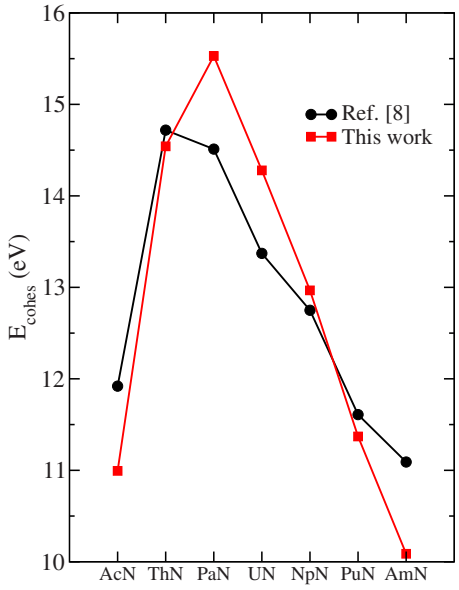

FIG. 4. (Color online) Cohesive energies of the actinide mononitrides.

electrons were largely localized. The XPS core-level spectrum of the Am metal film indicated some residual 5*f* hybridization, fairly suppressed in the Am compound films, and they categorized AmN and Am_2O_3 to be insulators but AmSb as a quasigap material. On the other hand, it is well known that spin polarization leads to partial electron localization, and for certain compounds this results in a much better agreement of computed equilibrium lattice parameters with experiments as opposed to non-spin-polarized computations (for AmN, this has been pointed out by Brooks,[10] and the effects can be clearly seen in Table II). However, this leads to the old problem of theory contradicting with experiment, as far as the magnetic structure of the ground state is concerned.[40] For AmN, one experimental study predicts temperature independent paramagnetism.[19] However, our calculations clearly predict a ferromagnetic ground state. A total spin moment of $5.64\mu_B$ is reported in Table II. From Table V, we observe a small orbital magnetic moment contribution, leading to a total site magnetic moment of $4.33\mu_B$.

We now discuss the electronic structures of the actinide compounds by focusing on the angular momentum decomposed (partial) density of states (DOS) inside the muffin tin for the *f* and *d* states for actinides and the *p* states of N. Only

TABLE V. Site-projected spin magnetic moment *S* (in μ_B), orbital magnetic moment *L* (in μ_B), and total magnetic moment (in μ_B) inside the muffin tin for the actinide atoms in the lowest energy structure of AnN with a magnetic ground state.

An	*S*	*L*	Total
U	0.86	−0.85	0.01
Np	2.26	−2.21	0.05
Pu	3.97	−2.16	1.81
Am	5.34	−1.01	4.33

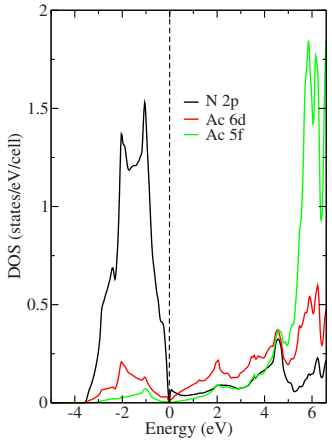

FIG. 5. (Color online) Partial DOS for AcN. The vertical line through $E=0$ is the Fermi level.

the lowest energy structures with the inclusion of SOC were considered, and for spin-polarized calculations, partial DOSs for each angular momentum were summed over spins. In Fig. 5, we show the partial DOS for AcN. From about −4.0 eV up to the Fermi level, we clearly observe N 2*p* and Ac 6*d* hybridizations and very small mixing with Ac 5*f* states. Also, there is a very small density of states at the Fermi level. The character and admixture of the Th 6*d* and N 2*p* states below the Fermi level for ThN shown in Fig. 6 is similar to the plot in Fig. 5 for AcN. Again, we observe a small contribution to the DOS by the 5*f* states and a small DOS at the Fermi level. In Fig. 7, we show the partial DOS for PaN. The Pa-N interaction is dominated Pa 6*d*, Pa 5*f*, and N 2*p* hybridizations. However, we also note an appreciable density of 5*f* states in the in the valence region near the Fermi level. In Fig. 8, we depict the partial DOS for UN. Compared to Ac, Th, and Pa, we clearly observe a significant density of states at the Fermi level and significant U(5*f*)-N(2*p*), U(6*d*)-N(2*p*), and U(5*f*)-U(6*d*) hybridizations. The partial DOS for NpN, PuN, and AmN are reported in Figs. 9–11, respectively. The N 2*p* hybridizations with the respective actinide 5*f* and 6*d* states and weak actinide 5*f*-6*d*

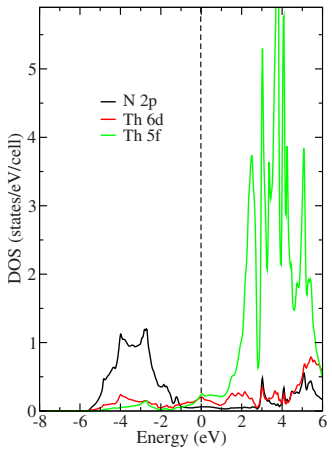

FIG. 6. (Color online) Partial DOS for ThN. The vertical line through $E=0$ is the Fermi level.

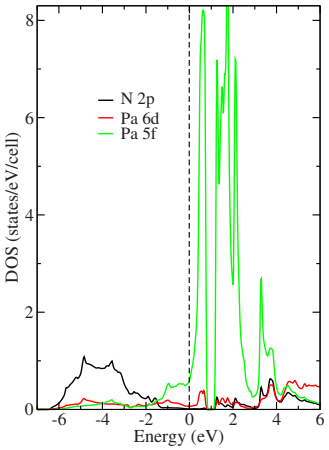

FIG. 7. (Color online) Partial density of states for PaN. The Fermi level is the vertical line through $E=0$.

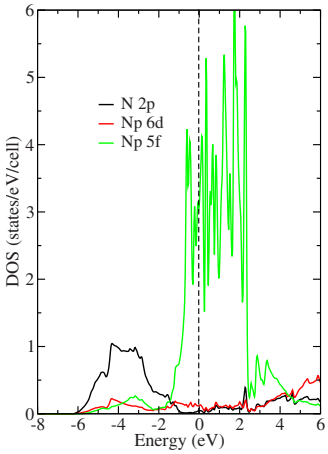

FIG. 9. (Color online) Partial density of states for NpN. The Fermi level is the vertical line through $E=0$.

hybridizations are noted. As stated before, recent photoemission experiments by Gouder *et al.*[39] clearly indicated that AmN is semiconductor, with Am $5f$ and N $2p$ states occurring at binding energies of 2.5 and 3.8 eV, respectively. The DOS for AmN reported in Fig. 11 predict Am $5f$ and N $2p$ binding energies of about 1.9 and 3.0 eV, respectively, whereas recent LDA+U calculations by Ghosh *et al.*[22] yielded binding energies of 2.5 eV (Am $5f$) and 3.0 eV (N $2p$). The LDA predicted pseudogaplike behavior and LDA+U predicted semiconducting behavior with a real gap of 192 meV observed by Ghosh *et al.*[22] have not been observed in our DOS for AmN.

One noticeable feature in the partial DOS is the gradual increase in the density of $5f$ states and the appearance peaks below the Fermi level from Pa to Am, all of which have nonempty $5f$ orbitals. The $5f$ DOS for Pa is relatively small below and at the Fermi level. For U $5f$ partial DOS in Fig. 8, we see a small peak just above the Fermi level. For Np $5f$ partial DOS in Fig. 9, we clearly see a single peak below the Fermi level, while for the $5f$ partial DOS for Pu in Fig. 10, we see a peak at around −1.8 eV and one peak just below the Fermi level. For the Am $5f$ DOS in Fig. 11, we notice an appreciable band width of about 2 eV, with a peak at around 2 eV and two more peaks just below the Fermi level. For pure Pa, U, and Np $5f$ states, it is well known that the $5f$ states are delocalized, and the same trend is manifested in the partial DOS for PaN, UN, and NpN. Similarly, the Pu and Am $5f$ peaks we have observed here are similar to the behavior in their pure states; hence, it may be interpreted as a sign of $5f$ electron localization.

The partial DOS was computed solely within the muffin tins and do not tell us anything about the interaction in the interstitial region. To further elucidate the nature of the interaction between the actinide metal and N, we computed the difference charge density, which gives us information about the nature of the chemical bonds formed as result of charge redistribution. We define the difference charge density $\Delta n(r)$ as follows:

$$\Delta n(r) = n(\mathrm{AnN}) - n(\mathrm{An}) - n(\mathrm{N}),$$

where $n(\mathrm{AnN})$ is the total charge density of the AnN solid, $n(\mathrm{An})$ is the total charge density of the actinide metal atom,

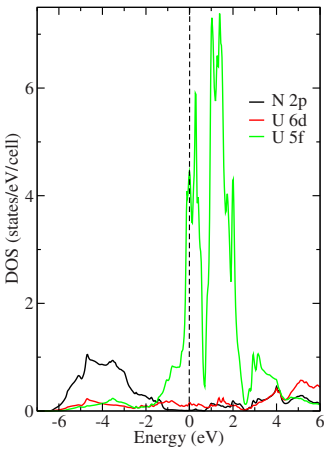

FIG. 8. (Color online) Partial DOS for UN. The vertical line through $E=0$ is the Fermi level.

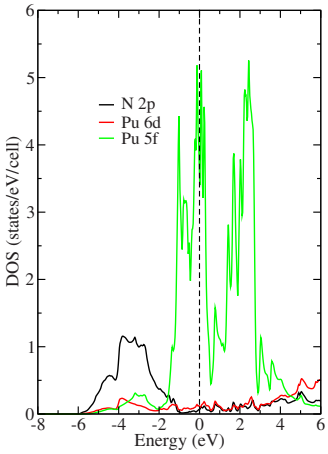

FIG. 10. (Color online) Partial density of states for PuN. The Fermi level is the vertical line through $E=0$.

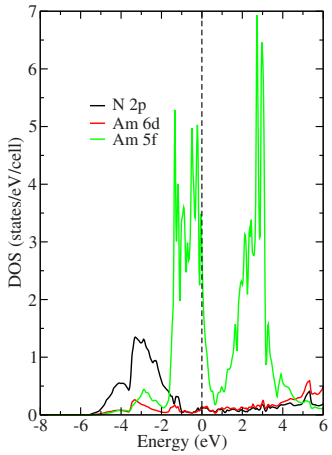

FIG. 11. (Color online) Partial density of states for AmN. The Fermi level is the vertical line through $E=0$.

and n(N) is the total charge density of the N atom. Furthermore, the An and N atoms remained at exactly the same positions as they were in the solid. In Fig. 12, we show the difference density plots for all the compounds. The density was computed in the (001) plane, and the coloring scheme and scale are indicated in the figure. In general, we observe charge accumulation around N and charge depletion around the actinide atoms. This clearly suggests that there is charge transfer from the actinide to N, indicating that the An-N chemical bonds are primarily ionic in character. This is expected since the N atom is more electronegative than the metal actinide atoms. Looking at the difference density plots for UN, NpN, PuN, and AmN in Fig. 12, charge depletion around the actinide atoms can be clearly observed. However, this is not the case for AcN, ThN, and PaN. For PaN, in particular, which is most stable in terms of cohesive energy, we see, in addition to regions of charge loss, small regions of charge gain around Pa, which we attribute to the extra contribution of covalent bonding to ionic bonding. For the other solids, we do not clearly see signs of covalent bonding. This might be due to the fact that covalent features of the bonds may be quite subtle and are not easily captured by difference density plots.

We also attempted to calculate the electronic specific heat coefficient γ by using an approximate model. For noninteracting electrons, the electronic specific heat coefficient γ is proportional to the total density of states $N(E_F)$ at the Fermi level and is given by $\gamma=(\pi^2/3)N(E_F)K_B^2$. For ThN, our estimated value of 2.64 mJ/(mol K^2) is comparable to the experimental value of 3.12 mJ/(mol K^2) (Ref. 30) and a recent FP-LAPW+lo with the GGA calculation,[20] which yielded a value of 2.74 mJ/(mol K^2). But for UN and PuN, we observe a large discrepancy between our estimated values and experimental data. To match the theoretical electronic specific heat coefficient γ to experimental values (Table VI), it should be corrected as γ(corrected)$=\gamma$(band)$^*(1+\lambda)$, where the parameter λ takes into account the electron-phonon interactions and many body effects, and γ(band) is our computed value.[43] We intend to pursue such studies in the future.

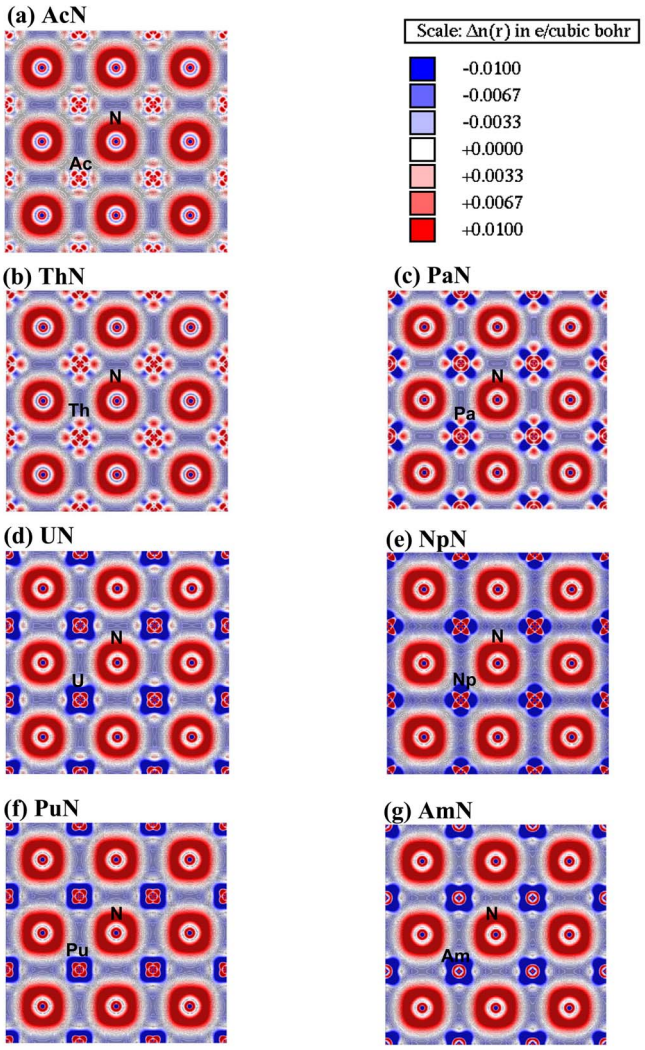

FIG. 12. (Color online) Difference electron density plots for (a) AcN, (b) ThN, (c) PaN, (d) UN, (e) NpN, (f) PuN, and (g) AmN computed in the (001) plane. Atoms are labeled accordingly, and the scale used is indicated at the top.

IV. CONCLUSIONS

The FP-LAPW+lo method has been used to systematically study the zero temperature structural and electronic properties of AnN (An=Ac, Th, Pa, U, Np, Pu, and Am). Each compound has been studied at the NM, FM, AFM configurations, all with and without SOC. The optimized lattice

TABLE VI. Electronic specific heat coefficient γ (in mJ mol^{-1} K^{-2}) computed using the free electron model and the corresponding experimental values.

	AcN	ThN	PaN	UN	NpN	PuN	AmN
Computed γ	0.12	2.64	2.36	13.5	8.69	9.30	8.06
Experimental γ		3.12[a]		25.0[b]		66.0[c]	

[a]Reference 30.
[b]Reference 41.
[c]Reference 42.

constants and bulk moduli for the lowest energy structures are in good agreement with known experimental data. The ground states of AcN, ThN, and PaN are clearly nonmagnetic, while the ground states of UN, NpN, PuN, and NpN are found to be ferromagnetic. Our zero temperature ferromagnetic structures predicted for UN, PuN, and AmN contradict experimental results, whereas both the ferromagnetic structure of NpN and the nonmagnetic structure of ThN agree with experiment. A study of the site-projected magnetic moments shows a cancellation of the spin and orbital moment behaviors for U and Np and of the localized magnetic moment for Pu and Am. A study of the partial density of states showed An $6d$ and N $2p$ hybridizations, with some admixture from PaN, UN, PuN, and AmN $5f$ electrons and also a $5f$ electron delocalization for Pa, U, and Np and a $5f$ localization for Pu and Am. The observed chemical bonding between the actinides and nitrogen has a significant ionic character. The specific heat coefficients have been computed using the free electron model. Further experimental and theoretical work needs to be done to clarify the discrepancies with measured magnetic structures for UN, PuN, and AmN and also thermal properties such as electronic specific heat coefficients. This could imply going beyond the techniques of standard density functional theory, but it is not clear at this point that this will necessarily solve the discrepancies.

ACKNOWLEDGMENTS

This work is supported by the Chemical Sciences, Geosciences and Biosciences Division, Office of Basic Energy Sciences, Office of Science, U.S. Department of Energy (Grant No. DE-FG02-03ER15409) and by the Welch Foundation, Houston, TX (Grant No. Y-1525).

*akr@uta.edu

[1] J. J. Katz, G. T. Seaborg, and L. R. Morss, *The Chemistry of the Actinide Elements* (Chapman and Hall, London, 1986).

[2] *Transuranium Elements: A Half Century*, edited by L. R. Morss and J. Fuger (American Chemical Society, Washington, D.C. 1992).

[3] *The Chemistry of the Actinide and Transactinide Elements*, edited by L. R. Morss, N. M. Edelstein, J. Fuger, and J. J. Katz (Springer, New York, 2006), Vols. 1–5.

[4] *Actinides—Basic Science, Applications, and Technology*, edited by L. Soderholm, J. J. Joyce, M. F. Nicol, D. K. Shuh, and J. G. Tobin, MRS Symposia Proceedings No. 802 (Materials Research Society, Pittsburgh, 2004).

[5] *Actinides 2005: Basic Science, Applications, and Technology*, edited by J. L. Sarrao, A. J. Schwartz, M. R. Antonio, P. C. Burns, R. G. Haire, and H. Nitsche, MRS Symposia Proceedings No. 893 (Materials Research Society, Pittsburgh, 2005).

[6] D. A. Young, *Phase Diagrams of the Elements* (University of California Press, Berkeley, 1991).

[7] International Nuclear Societies Council, Technical Report, 1996 (unpublished).

[8] D. Sedmidubsky, R. J. M. Konings, and P. Novak, J. Nucl. Mater. **344**, 40 (2005).

[9] R. Atta-Fynn and A. K. Ray, Physica B **392**, 112 (2007); Phys. Rev. B **75**, 195112 (2007), and references therein.

[10] M. S. S. Brooks and P. J. Kelly, Phys. Rev. Lett. **51**, 1708 (1983); M. S. S. Brooks, J. Phys. F: Met. Phys. **14**, 857 (1984).

[11] K. Kurosaki, J. Adachi, M. Uno, and S. Yamana, J. Nucl. Mater. **344**, 45 (2005).

[12] L. Petit, A. Svane, W. M. Temmerman, and Z. Szotek, Phys. Rev. B **63**, 165107 (2001); Eur. Phys. J. B **24**, 139 (2002).

[13] L. Havela, F. Wastin, J. Rebizant, and T. Gouder, Phys. Rev. B **68**, 085101 (2003); D. Rafaja, L. Havela, R. Kuzel, F. Wastin, E. Colineau, and T. Gouder, J. Alloys Compd. **386**, 87 (2005).

[14] M. Marutzky, U. Barkow, J. Schoenes, and R. Troć, J. Magn. Magn. Mater. **299**, 225 (2006).

[15] J. Sheng, J. Mater. Sci. Lett. **20**, 1757 (2001).

[16] D. A. Sverjensky and P. A. Molling, Nature (London) **356**, 231 (1992); D. A. Sverjensky, *ibid.* **358**, 310 (1992).

[17] K. Schwarz, P. Blaha, and G. K. H. Madsen, Comput. Phys. Commun. **147**, 71 (2002); P. Blaha, K. Schwarz, G. K. H. Madsen, D. Kvasnicka, and J. Luitz, *WIEN2K, An Augmented Plane Wave+Local Orbitals Program for Calculating Crystal Properties* (Technische Universität Wien, Austria, 2001).

[18] J. P. Perdew, K. Burke, and M. Ernzerhof, Phys. Rev. Lett. **77**, 3865 (1996).

[19] Inorganic Crystal Structure Database, Version 1.3.1, FIZ Karlsruhe, 2003.

[20] I. R. Shein, K. I. Shein, and A. L. Ivanovskii, J. Nucl. Mater. **353**, 19 (2006).

[21] A. O. Shorikov, A. V. Lukoyanov, M. A. Korotin, and V. I. Anisimov, Phys. Rev. B **72**, 024458 (2005).

[22] D. B. Ghosh, S. K. De, P. M. Oppeneer, and M. S. S. Brooks, Phys. Rev. B **72**, 115123 (2005).

[23] D. D. Koelling and B. N. Harmon, J. Phys. C **10**, 3107 (1977).

[24] J. Kunes, P. Novak, R. Schmid, P. Blaha, and K. Schwarz, Phys. Rev. B **64**, 153102 (2001).

[25] A. Zunger, J. P. Perdew, and G. L. Oliver, Solid State Commun. **34**, 933 (1980); J. P. Perdew and A. Zunger, Phys. Rev. B **23**, 5048 (1981).

[26] W. M. Temmerman, A. Svane, Z. Szotek, and H. Winter, in *Electronic Density Functional Theory: Recent Progress and New Directions*, edited by J. F. Dobson, G. Vignale, and M. P. Das (Plenum, New York, 1998), p. 327.

[27] F. D. Murnaghan, Proc. Natl. Acad. Sci. U.S.A. **30**, 244 (1944).

[28] O. Vogt and K. Mattenberger, J. Alloys Compd. **223**, 226 (1995).

[29] *Handbook of the Physics and Chemistry of the Actinides*, edited by A. J. Freeman and G. H. Lander (North-Holland, Amsterdam, 1985).

[30] R. Benz and A. Naoumidis, *Thorium Compounds with Nitrogen, Gmelin Handbook of Inorganic Chemistry*, 8th ed. (Springer, Berlin, 1987), Thorium supplement, Vol. C3.

[31] N. A. Curry, Proc. Phys. Soc. London **86**, 1193 (1965).

[32] R. Troć, J. Solid State Chem. **13**, 14 (1975).

[33] P. De V. Du Plessis and C. F. Van Doorn, Physica B & C **86**, 993 (1977).

[34] T. M. Holden, W. J. L. Buyers, E. C. Svensson, J. A. Jackmann, A. F. Murray, O. Vogt, and P. De V. Du Plessis, J. Appl. Phys. **53**, 1967 (1982).
[35] A. T. Aldred, B. D. Dunlap, A. R. Harvey, D. J. Lam, G. H. Lander, and M. H. Muller, Phys. Rev. B **9**, 3766 (1974).
[36] A. Bouef, R. Cacciuffo, J. M. Fournier, L. Manes, J. Rebizant, E. Roudant, and F. Rustichelli, Solid State Commun. **52**, 451 (1984).
[37] D. J. Martin, R. D. A. Hall, J. A. Lee, M. J. Mortimer, and P. W. Sutcliffe, Harwell AERE Rep. **76**, 12599 (1976).
[38] H. L. Skriver, O. K. Andersen, and B. Johansson, Phys. Rev. Lett. **41**, 42 (1978); **44**, 1230 (1980).
[39] T. Gouder, P. M. Oppeneer, F. Huber, F. Wastin, and J. Rebizant, Phys. Rev. B **72**, 115122 (2005); J. R. Naegele, L. Manes, J. C. Spirlet, and W. Müller, Phys. Rev. Lett. **52**, 1834 (1984).
[40] D. Gao and A. K. Ray, Eur. Phys. J. D **55**, 13 (2007).
[41] J. O. Scarbrough, H. L. Davis, W. Fulkerson, and J. O. Betterton, Phys. Rev. **176**, 666 (1968).
[42] R. O. A. Hall, J. A. Lee, D. J. Martin, M. J. Mortimer, and P. W. Sutcliffe, J. Chem. Thermodyn. **10**, 935 (1978).
[43] M. B. Brodsky, Rep. Prog. Phys. **41**, 1547 (1978).